Higher order adaptively integrated cohesive element

Russo, Raffaele; Chen, Boyang

Publication date
2020

Document Version
Final published version

Published in
ECCM 2018 - 18th European Conference on Composite Materials

HIGHER ORDER ADAPTIVELY INTEGRATED COHESIVE ELEMENT

Raffaele Russo[1] and Boyang Chen[2]

Faculty of Aerospace Engineering, Delft University of Technology,
Kluyverweg 1, 2629 HS Delft, the Netherlands
[1]Email: r.russo-1@student.tudelft.nl
[2]Email: B.Chen-2@tudelft.nl

Keywords: Delamination, Fracture Mechanics, Cohesive Element, Cohesive Zone Modelling.

Abstract
Cohesive Element (CE) is a well-established finite element for fracture, widely used for the modelling of delamination in composites. However, the computational time of CE-based method is prohibitive. This is because the steep and non-smooth stress gradient in the cohesive zone requires a very fine mesh. In this context, a new type of CE is here proposed, aiming to loosen the mesh constraint and reduce the computational time. It uses a higher-order interpolation of the displacement field with rotational degree of freedom and an adaptive integration scheme based on the status of the element. The proposed CE has been validated through comparison with benchmark solutions of delamination in Mode I, Mode II and Mixed-Mode cases, and has demonstrated superior performance than standard CE in computational efficiency while retaining a high level of accuracy.

1. Introduction

CE, which is based on CZM [1, 2], is one of the most popular methods for the modelling of delamination. CZM assumes that traction exists between the crack surfaces. This traction is a function of the crack opening and a damage variable which represents the loss of stiffness. Camanho et al. developed the CE which has been widely adopted to model delamination in composites [3]. Turon et al. subsequently refined their formulation by defining a thermodymically consistent damage model to ensure congruity between damage initiation and propagation [4]. These CEs use linear shape functions to interpolate the displacement field, and hence also the crack opening. The main limitation of the linear CEs lies in the restriction on the element size to ensure solution accuracy [5, 6, 7, 8, 9, 10, 11, 12, 13]. A steep and non-smooth stress gradient is present in the cohesive zone (Figure 1), and the mesh must be dense enough to catch the stress variation within it. In general, there needs to be at least three elements within the Cohesive Zone Length (CZL) to capture the stress gradient [7, 3, 5]. During crack propagations, the cohesive zone moves, thereby extending this constraint to all the CEs.

The mesh constraint limits the application of CEs on large-scale structures. Several solutions to tackle this issue have been proposed by different authors. Turon et al. lowered the strengths of the CE to enlarge the CZL, thereby allowing larger elements to be used [14]. Yang et al. [8] and Do et al. [11] proposed a sub-domain Gaussian integration scheme for first-order CEs. Alvarez et al. introduced a 6-node 2D CE to interpolate the displacement field with quadratic shape functions [13]. Samimi et al. enriched the standard linear shape functions with triangular bilinear function to adaptively model the moving cohesive zone [15]. Guiamatsia et al. employed the analytical solution of the displacement field for a beam on elastic foundation under Mode I loading as enrichment functions to the CE shape functions [16]. Lu et al. used the floating node method to adaptively partition a large linear CE into small sub-CEs when the cohesive zone is passing through [17].

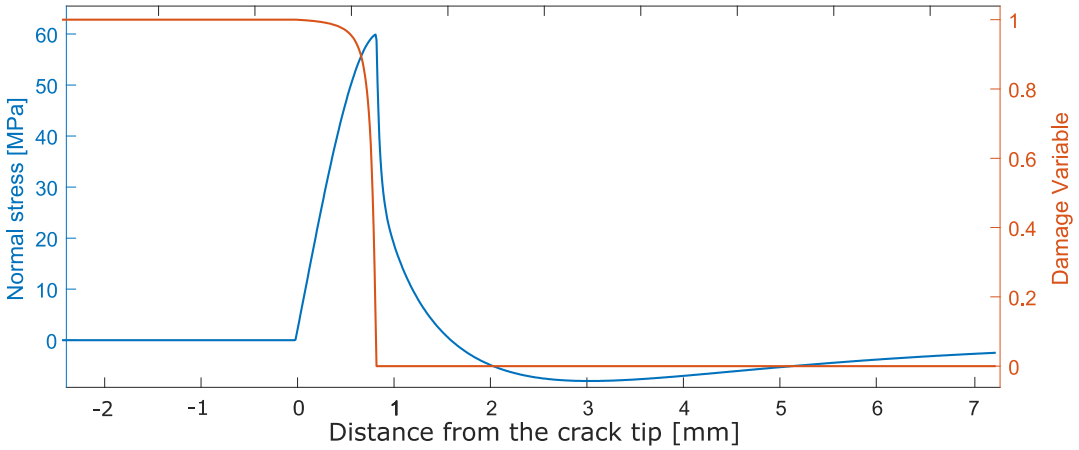

Figure 1. Normal stress distribution near the crack tip in a Double Cantilever Beam test.

2. Proposed Method

2.1 Displacement interpolation

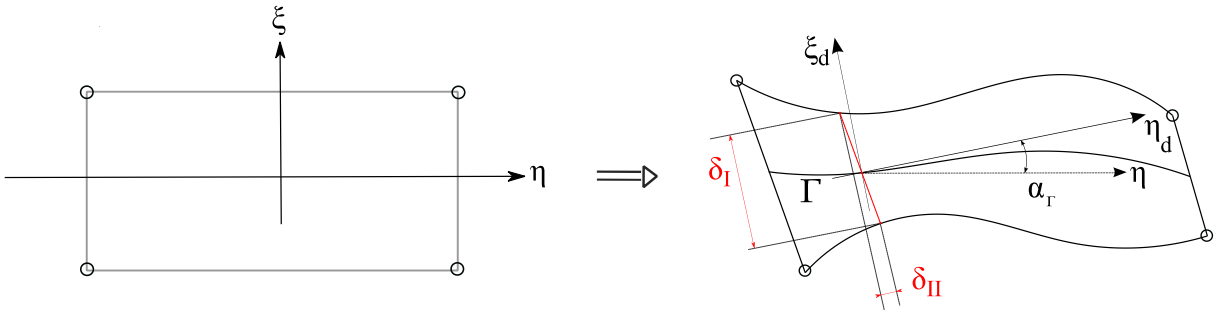

Figure 2. Visualization of un-deformed (left) and deformed (right) configuration of the proposed CE.

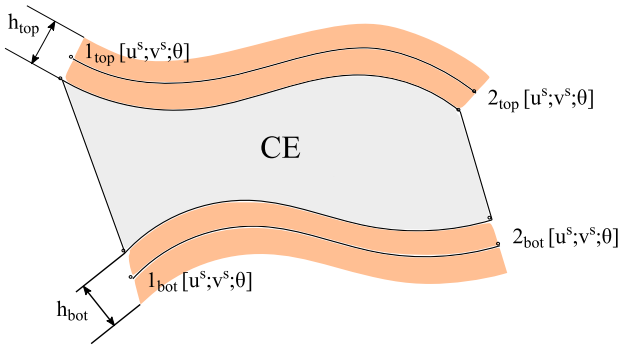

Figure 3. Application of the proposed CE together with EB beam elements.

In this work, a new third-order CE with rotational degree of freedom is proposed. It is designed to be used between Euler-Bernoulli (EB) beam elements. Figure 2 depicts the proposed CE. Each node possesses three degree of freedom, two translational and one rotational. The rotational degree of freedom ensures compatibility with the EB beam elements and the C^1 continuity of the displacement field between adjacent CEs. The displacements of the top and bottom edges (subscripted by 'top' and 'bot', respectively) of the new CE are described by Equations 1 and 2, respectively:

$$u_{\text{top}}(\eta) = u^{\text{s}}_{\text{top}}(\eta) - \frac{h_{\text{top}}}{2}\sin(\theta_{\text{top}}) \qquad v_{\text{top}}(\eta) = v^{\text{s}}_{\text{top}}(\eta) + \frac{h_{\text{top}}}{2}\left[1 - \cos(\theta_{\text{top}})\right] \tag{1}$$

$$u_{\text{bot}}(\eta) = u^{\text{s}}_{\text{bot}}(\eta) + \frac{h_{\text{bot}}}{2}\sin(\theta_{\text{bot}}) \qquad v_{\text{bot}}(\eta) = v^{\text{s}}_{\text{bot}}(\eta) - \frac{h_{\text{bot}}}{2}\left[1 - \cos(\theta_{\text{bot}})\right] \tag{2}$$

where h is the thickness of the beam, $u^{\text{s}}, v^{\text{s}}$ and θ are the horizontal, vertical and rotational degrees of freedom of the neutral axis, respectively.

2.2 Computing the openings

With the above expressions of displacements for the top and bottom edges, the normal and shear openings of the proposed CE can be computed in the un-deformed frame of reference $\{\eta, \xi\}$ as follows:

$$\boldsymbol{\delta} = \left[v_{\text{top}} - v_{\text{bot}}, \qquad u_{\text{top}} - u_{\text{bot}}\right]^{\text{T}} \tag{3}$$

As the CE is third order, the mid-line of the CE becomes curved after deformation. In this formulation, the openings are rotated with respect to the current orientation of the CE mid-line (α_Γ in Figure 2), i.e., they are expressed in the deformed frame of reference $\{\eta_{\text{d}}, \xi_{\text{d}}\}$. Following the definition of the mid-line, a parameterized description of the CE domain (Γ) in the un-deformed frame of reference can be obtained, from which the rotation angle α_Γ can be calculated. The angle α_Γ and the differential of the domain ($\text{d}\Gamma$) are:

$$\alpha_\Gamma(\eta) = \arctan\left(\frac{\dfrac{\partial \Gamma_\eta}{\partial \eta}}{\dfrac{\partial \Gamma_\xi}{\partial \eta}}\right) \qquad \text{d}\Gamma(\eta) = \sqrt{\left(\frac{\partial \Gamma_\eta}{\partial \eta}\right)^2 + \left(\frac{\partial \Gamma_\xi}{\partial \eta}\right)^2}\,\text{d}\eta = J\,\text{d}\eta \tag{4}$$

Once α_Γ is obtained, the opening can be rotated to the deformed frame of reference as follows:

$$\boldsymbol{\delta}_{\text{d}} = \begin{bmatrix}\delta_{\text{I}} \\ \delta_{\text{II}}\end{bmatrix} = \boldsymbol{\Phi}\,\boldsymbol{\delta}\,, \text{ where } \boldsymbol{\Phi} = \begin{bmatrix}\cos(\alpha_\Gamma) & \sin(\alpha_\Gamma) \\ -\sin(\alpha_\Gamma) & \cos(\alpha_\Gamma)\end{bmatrix} \tag{5}$$

2.3 Integration Procedure

From the virtual work principle, we have:

$$\int_\Gamma \delta\boldsymbol{\delta}_{\text{d}}^{\text{T}}\,\boldsymbol{\tau}\,\text{d}\Gamma = \delta\mathbf{q}^{\text{T}}\int_\Gamma \mathbf{B}^{\text{T}}\,\mathbf{D}(d)\,\boldsymbol{\delta}_{\text{d}}\,\text{d}\Gamma = \delta\mathbf{q}^{\text{T}}\,\mathbf{F}_{\text{ext}} \tag{6}$$

Where $\boldsymbol{\tau}$ is the traction vector, $\delta\boldsymbol{\delta}_{\text{d}} = \mathbf{B}\,\delta\mathbf{q}$, $\mathbf{q}$ is the nodal degree of freedom vector of the CE, and $\boldsymbol{\tau} = \mathbf{D}(d)\,\boldsymbol{\delta}_{\text{d}}$, $\mathbf{D}(d)$ is the cohesive stiffness matrix which is a function of the damage variable according the cohesive law. The tangent stiffness matrix of the CE is approximated by the material tangent stiffness matrix:

$$\mathbf{K} = \int_{-1}^{1} \mathbf{B}^{\text{T}}\,\mathbf{D}(d)\,\mathbf{B}\,J\,\text{d}\eta \tag{7}$$

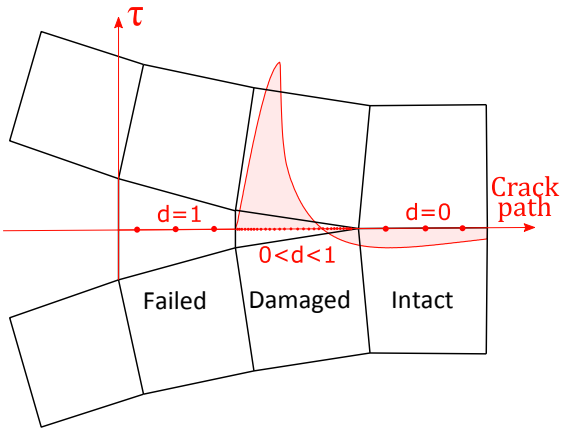

Figure 4. Adaptively Gaussian integration scheme. The red dots indicate the integration points.

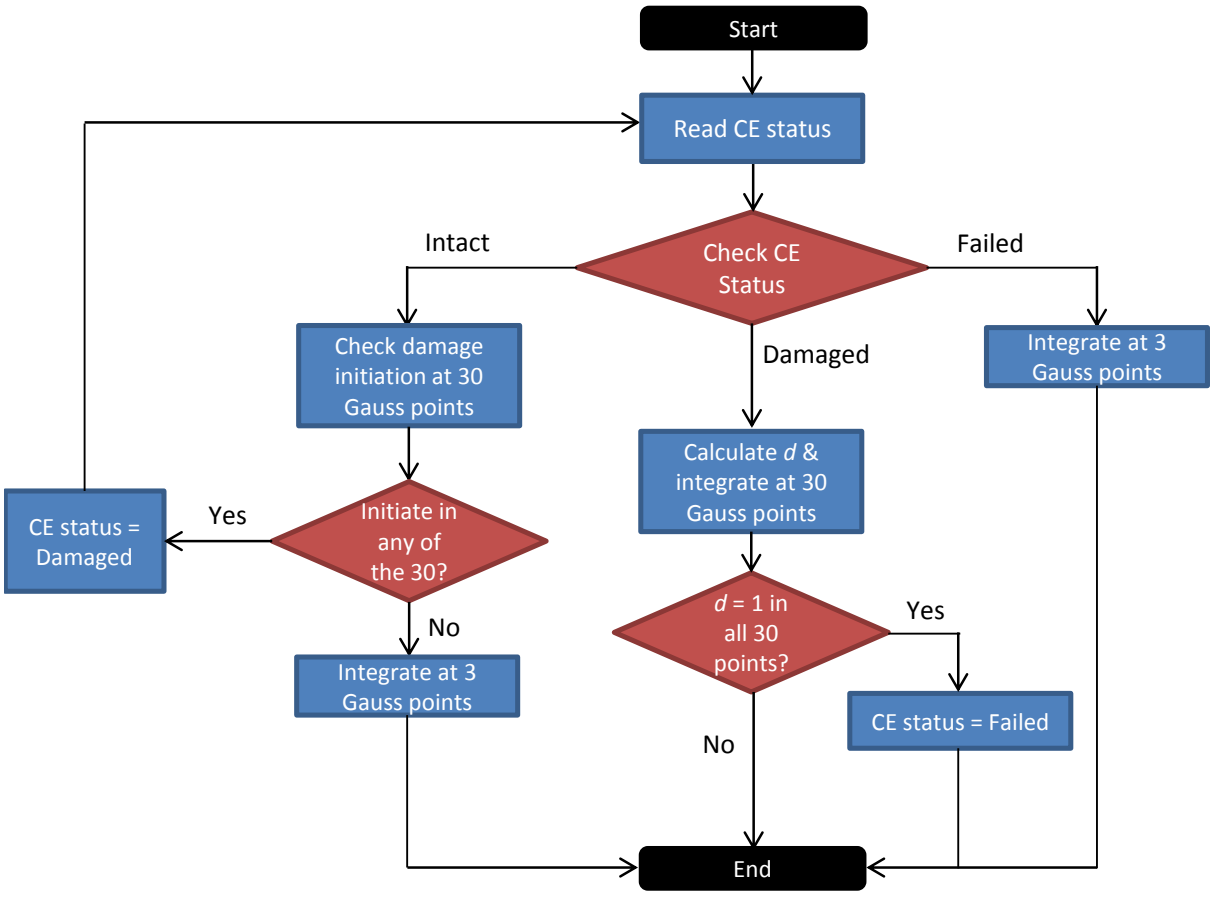

Figure 5. Flowchart of adaptive integration

An adaptive integration scheme is proposed for the new CE, which depends on the status of the CE. The CE status can be intact ($d = 0$ throughout), damaged ($0 < d < 1$ in certain locations) or failed (d = 1 throughout), as shown in Figure 4. Figure 5 illustrates the adaptive procedure. If $d = 0$ at all 30 points, the element is linear-elastic and only 3 Gauss points are used for subsequent integration. If $d > 0$ in any of the 30 points, then the cohesive zone is travelling across this element and all 30 Gauss

points are used for subsequent integration. If $d = 1$ in all 30 points (complete failure of the CE), then the integration is revert back to the simple 3-point scheme for fast calculation.

3 Validation

The new CE has been tested under pure Mode I, Mode II and 50% Mixed Mode, through the simulation of the Double Cantilever Beam (DCB), End-Notched Flexure (ENF) and Mixed-Mode Bending (MMB) tests respectively. The load-displacement curves have been extracted from the performed tests. The analytical solutions of the load-displacements curves have been used to validate the CEs [9]. The material properties and geometry of the specimen for the DCB case have been taken from [14] and those of the ENF and the MMB cases from [9]. The penalty stiffness of the CE is 555 GPa/mm. The mode I material strength is 60 MPa for DCB and 30 MPa for ENF and MMB. The methodology proposed by Turon et al. [9] has been used to compute the mode II material strength, which led to a value of 101.2 MPa for DCB and 58.9 MPa for ENF and MMB. For comparison, the benchmark cases have been modelled using plain strain elements (CPE4) and standard linear cohesive elements (COH2D4) in ABAQUS. Five elements through-the-thickness have been used for beams in DCB and ENF, and ten for MMB as the stress field is more complicated. A quadratic stress-based criterion has been used to identify the damage onset, and a bilinear cohesive law with the B-K mixed-mode formula has been used to define the damage evolution.

The results of load-displacement curves are presented in Figure 6. In DCB, the result of linear 0.25 mm CE model follows closely the experimental curve. However, with 2 mm and larger linear CEs, the results would be far off the experimental curve, as shown in Figure 6(a). The predicted peak load is 185% of the experimental value with 2.5-mm linear CE. With the new CE, with the 2.5-mm elements model, the peak load prediction is 104% of the analytical value and the predicted propagation curve follows closely the analytical one (Figure 6(b)). In the case of even larger CEs, linear CE model predicts no delamination within the duration of the simulation, while the 5-mm new CE model's peak load prediction is at 108% of the analytical value and the propagation curve still follows quite well the analytical one (Figure 6(b)). The stiffness of the new CE model is slightly larger than the analytical one, because the analytical solution is based on the corrected beam theory while the model is based on EB beam theory. The damage propagation phase is however not affected by this deviation. In ENF, similar observations can be made. the 2 mm and 5 mm linear CE models lead to an overshoot of the delamination onset by 115 % and 131%, respectively (Figure 6(c)). The 2 mm new CE model provides an excellent agreement with the analytical curve. The 5 mm new CE model is also able to predict the load-displacement curve quite accurately without huge overshoot of the peak load (Figure 6(d)). For the MMB case, the same conclusion can be reached. In the new CE model, the element size can be one order of magnitude larger than the one required for linear CEs and the load-displacement solution is equally, if not more, accurate (Figure 6(f)).

Some comparisons (Table 1) have been made between the standard CE simulations and those of the new CE with similar levels of accuracy. The solver control settings are kept constant. As expected, because of the use of much larger elements and overall much fewer number of integration points, the new CE models can achieve a significant amount of saving in all aspects of the comparison.

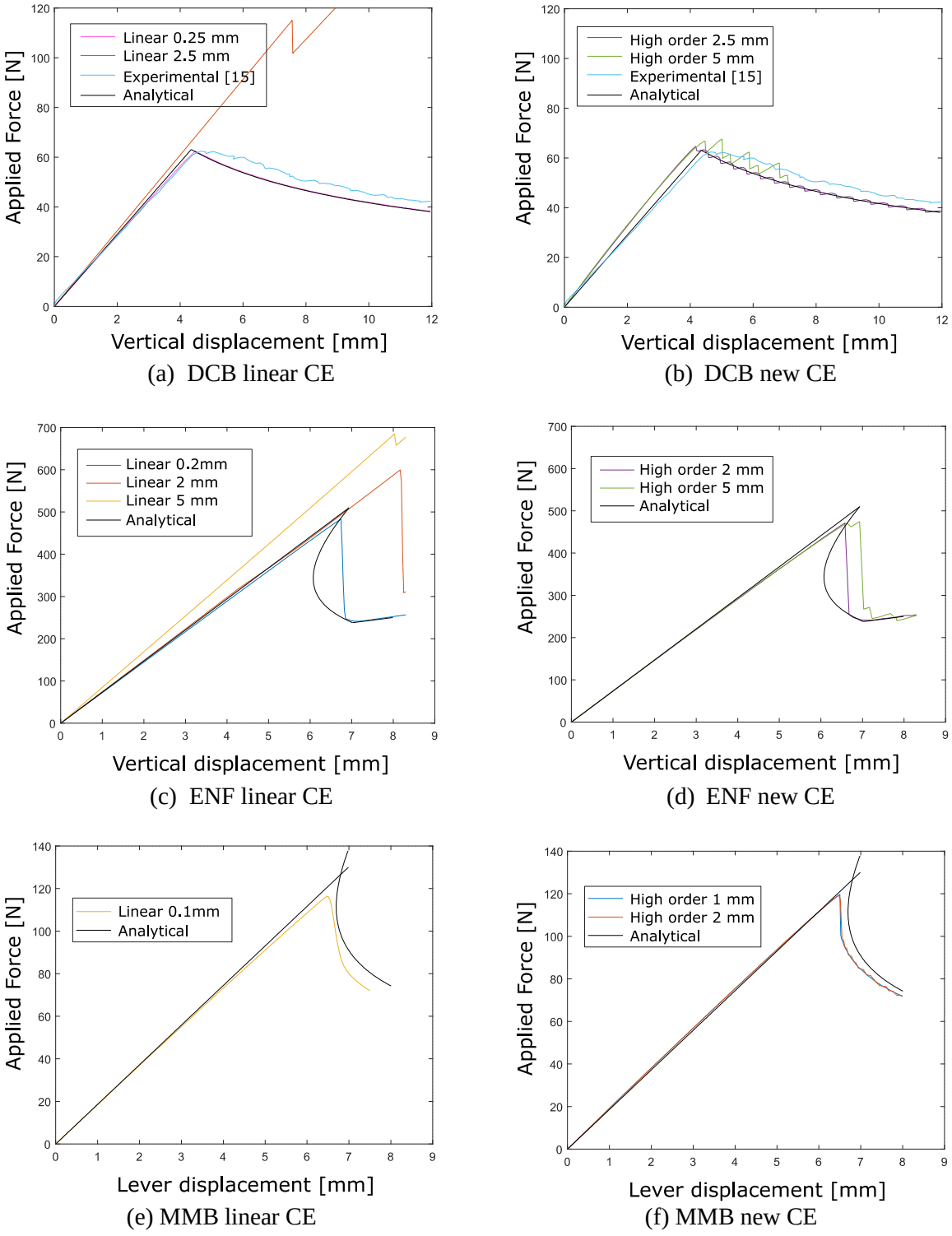

Figure 6. Comparison performances CEs DCB (a-b), ENF (c-d) and MMB (e-f).

Table 1. Cost comparison of simulations - new CE vs linear CE

	DCB		**ENF**		**MMB**	
	Standard 0.25 mm CE	High Order 2.5 mm CE	Standard 0.2 mm CE	High Order 2 mm CE	Standard 0.2 mm CE	High Order 2 mm CE
# Elements	8901	158	6765	208	26490	144
# D.o.F.	11040	606	15056	824	55847	1092
CPU Time	2606 s	47 s	4406 s	47 s	32759 s	55 s
Time/D.o.F.	0.236	0.077	0.292	0.057	0.589	0.050
# Iterations	7088	1123	4851	1123	16619	1380

4 Conclusions

In this paper a new adaptively integrated 3rd-order Cohesive Element has been presented. The proposed CE employs rotational degree of freedom and the 3rd order interpolation functions of Euler-Bernoulli beam elements. While the interpolation scheme remains fixed, the integration scheme adapts to the status of the CE, where a finer integration scheme is used when the cohesive zone is passing through the element domain. It has been demonstrated on DCB, ENF and MMB simulations that the proposed CE, as compared to linear CE, can give accurate predictions of the whole load-displacement curves with: 1) one order of magnitude larger elements; and 2) significantly reduced CPU time and number of iterations. Future work will be on the extension of the presented methodology on 3D cohesive elements.

References

[1] G. I. Barenblatt, "The Mathematical Theory of Equilibrium Cracks in Brittle Fracture," in *Advances in Applied Mechanics,* Elsevier, 1962, pp. 55-129.

[2] D. S. Dudgale, "Yielding of steel sheets containing slits," *Journal of the Mechanics and Physics of Solids,* vol. 8, pp. 100-104, 1960.

[3] P. Camanho and C. Davila, "Mixed-Mode Decohesion Finite Elements in for the Simulation Composite of Delamination Materials," *Nasa,* Vols. TM-2002-21, no. June, pp. 1-37, 2002.

[4] A. Turon, P. P. Camanho, J. Costa and C. G. Dávila, "A damage model for the simulation of delamination in advanced composites under variable-mode loading," *Mechanics of Materials,* vol. 38, pp. 1072-1089, 11 2006.

[5] Q. Yang and B. Cox, "Cohesive models for damage evolution in laminated composites," *International Journal of Fracture,* vol. 133, pp. 107-137, 5 2005.

[6] A. Turon, J. Costa, P. P. Camanho and C. G. Dávila, "Simulation of delamination in composites under high-cycle fatigue," *Composites Part A: Applied Science and Manufacturing,* vol. 38, pp. 2270-2282, 2007.

[7] P. W. Harper and S. R. Hallett, "Cohesive zone length in numerical simulations of composite delamination," *Engineering Fracture Mechanics,* vol. 75, pp. 4774-4792, 11 2008.

[8] Q. D. Yang, X. J. Fang, J. X. Shi and J. Lua, "An improved cohesive element for shell delamination analyses," *International Journal for Numerical Methods in Engineering,* 2010.

[9] A. Turon, P. P. Camanho, J. Costa and J. Renart, "Accurate simulation of delamination growth under mixed-mode loading using cohesive elements: Definition of interlaminar

strengths and elastic stiffness," *Composite Structures,* vol. 92, pp. 1857-1864, 2010.

[10] P. W. Harper, L. Sun and S. R. Hallett, "A study on the influence of cohesive zone interface element strength parameters on mixed mode behaviour," *Composites Part A: Applied Science and Manufacturing,* vol. 43, pp. 722-734, 2012.

[11] B. C. Do, W. Liu, Q. D. Yang and X. Y. Su, "Improved cohesive stress integration schemes for cohesive zone elements," *Engineering Fracture Mechanics,* vol. 107, pp. 14-28, 2013.

[12] B. Li, Y. Li and J. Su, "A combined interface element to simulate interfacial fracture of laminated shell structures," *Composites Part B: Engineering,* vol. 58, pp. 217-227, 2014.

[13] D. Álvarez, B. R. K. Blackman, F. J. Guild and A. J. Kinloch, "Mode I fracture in adhesively-bonded joints: A mesh-size independent modelling approach using cohesive elements," *Engineering Fracture Mechanics,* vol. 115, pp. 73-95, 2014.

[14] A. Turon, C. G. Dávila, P. P. Camanho and J. Costa, "An engineering solution for mesh size effects in the simulation of delamination using cohesive zone models," *Engineering Fracture Mechanics,* vol. 74, pp. 1665-1682, 2007.

[15] M. Samimi, J. A. W. Van Dommelen and M. G. D. Geers, "A self-adaptive finite element approach for simulation of mixed-mode delamination using cohesive zone models," *Engineering Fracture Mechanics,* vol. 78, pp. 2202-2219, 2011.

[16] I. Guiamatsia, G. A. O. Davies, J. K. Ankersen and L. Iannucci, "A framework for cohesive element enrichment," *Composite Structures,* vol. 92, pp. 454-459, 2010.

[17] X. Lu, B. Chen, V. Tan and T. Tay, "Adaptive floating node method for modelling cohesive fracture of composite materials," *Engineering Fracture Mechanics,* no. March, 2018.